

Potential flow of a second-order fluid over a sphere or an ellipse

By J. WANG AND D. D. JOSEPH

Department of Aerospace Engineering and Mechanics, University of Minnesota,
Minneapolis, MN 55455, USA

(Received 9 May 2003 and in revised form 10 March 2004)

We study the potential flow of a second-order fluid over a sphere or an ellipse. The normal stress at the surface of the body is calculated and has contributions from the inertia, viscous and viscoelastic effects. We investigate the effects of Reynolds number and body size on the normal stress; for the ellipse, various angles of attack and aspect ratios are also studied. The effect of the viscoelastic terms is opposite to that of inertia; the normal stress at a point of stagnation can change from compression to tension. This causes long bodies to turn into the stream and causes spherical bodies to chain. For a rising gas bubble, the effect of the viscoelastic and viscous terms in the normal stress is to extend the rear end so that it tends to the cusped trailing edge observed in experiments.

1. Introduction

Potential flows are solutions of the equations of motion for fluids which admit solutions with zero vorticity. For incompressible fluids with stresses given by

$$\mathbf{T} = -p\mathbf{1} + \boldsymbol{\tau}[\mathbf{u}], \quad (1.1)$$

this condition can be written as

$$\text{curl}(\nabla \cdot \mathbf{T}) = \text{curl}(\nabla \cdot \boldsymbol{\tau}[\nabla\phi]) = 0, \quad (1.2)$$

the divergence of the stress $\boldsymbol{\tau}[\nabla\phi]$ evaluated on irrotational flow is irrotational. Though this condition is not satisfied for $\mathbf{u} = \nabla\phi$ by most constitutive equations (Joseph & Liao 1994*a, b*), it is satisfied for inviscid fluid, for viscous fluid with constant properties, for linear viscoelastic and second-order fluids which will be discussed below.

The stress \mathbf{T} in an incompressible fluid of second grade is given by

$$\mathbf{T} = -p\mathbf{1} + \mu\mathbf{A} + \alpha_1\mathbf{B} + \alpha_2\mathbf{A}^2, \quad (1.3)$$

where $\mathbf{A} = \mathbf{L} + \mathbf{L}^T$ is the symmetric part of the velocity gradient $\mathbf{L} = \nabla\mathbf{u}$,

$$\mathbf{B} = \partial\mathbf{A}/\partial t + (\mathbf{u} \cdot \nabla)\mathbf{A} + \mathbf{A}\mathbf{L} + \mathbf{L}^T\mathbf{A}, \quad (1.4)$$

μ is the zero shear viscosity, $\alpha_1 = -n_1/2$ and $\alpha_2 = n_1 + n_2$ where $[n_1, n_2] = [N_1(\dot{\gamma}), N_2(\dot{\gamma})]/\dot{\gamma}^2$ as $\dot{\gamma} \rightarrow 0$ are the constants obtained from the first and second normal stress differences.

The equations of motion are $\text{div}\mathbf{u} = 0$ and

$$\rho[\partial\mathbf{u}/\partial t + (\mathbf{u} \cdot \nabla)\mathbf{u}] = -\nabla p + \mu\nabla^2\mathbf{u} + \text{div}[\alpha_1\mathbf{B} + \alpha_2\mathbf{A}^2]. \quad (1.5)$$

When $\mathbf{u} = \nabla\phi$ (see Joseph 1992a),

$$\begin{aligned} \operatorname{div}(\mathbf{u} \cdot \nabla \mathbf{A}) &= \operatorname{grad} \chi, & \operatorname{div}(\mathbf{A}\mathbf{L}) &= \operatorname{grad} \chi, & \operatorname{div} \mathbf{A}^2 &= 2\operatorname{grad} \chi \\ &\Rightarrow \operatorname{div}[\alpha_1 \mathbf{B} + \alpha_2 \mathbf{A}^2] &= \operatorname{grad}(3\alpha_1 + 2\alpha_2)\chi, \end{aligned} \quad (1.6)$$

where

$$\chi = \frac{\partial^2 \phi}{\partial x_i \partial x_j} \frac{\partial^2 \phi}{\partial x_j \partial x_i} = \frac{1}{4} \operatorname{tr} \mathbf{A}^2, \quad A_{ij} = 2 \frac{\partial^2 \phi}{\partial x_i \partial x_j}.$$

Combining (1.5) and (1.6) we find a Bernoulli equation

$$\rho \frac{\partial \phi}{\partial t} + \frac{1}{2} \rho |\nabla \phi|^2 + p - \hat{\beta} \chi = C(t), \quad (1.7)$$

where $\hat{\beta} = 3\alpha_1 + 2\alpha_2 \geq 0$ is the climbing constant. Returning now to the stress (1.3) with the pressure (1.7), we obtain

$$\mathbf{T} = - \left[C + \hat{\beta} \chi - \rho \frac{\partial \phi}{\partial t} - \frac{1}{2} \rho |\nabla \phi|^2 \right] \mathbf{1} + \left[\mu + \alpha_1 \left(\frac{\partial}{\partial t} + \mathbf{u} \cdot \nabla \right) \right] \mathbf{A} + (\alpha_1 + \alpha_2) \mathbf{A}^2. \quad (1.8)$$

The second-order fluid arises from an expansion of the general stress functional for slow and slowly varying motions, sometimes called retarded (Rivlin & Ericksen 1955; Bird, Armstrong & Hassager 1987; Joseph 1990). It has been used in many studies of viscoelastic behaviour with varying degrees of success; the predictions of fluid mechanic response to rapidly varying motions in which fluid memory is important have not been satisfactory, but the predictions for slow steady motions are excellent. We regard the results of analysis using the second-order fluid model as tentative and subject to ultimate validation by experiment and by comparison with direct numerical simulation using other constitutive equations.

Here, we consider the behaviour of a second-order fluid in irrotational steady flows which are otherwise unrestricted; the stresses in such flows do not vanish. In the case of irrotational flow of a viscous and viscoelastic fluid, the stresses can depend significantly on the viscosity and viscoelastic parameters. We are interested in the stresses on a body in a uniform stream. The continuity of the shear stress and tangential velocity on the boundary cannot be enforced in general in irrotational motions, though there are cases, like the flow near stagnation points where shears are not important (Joseph & Wang 2004). In looking to potential flow of a second-order fluid we are motivated by the fact that the irrotational normal stresses can produce viscous and viscoelastic torques on solid bodies and deformations of gas bubbles, which agrees with observations. It is, of course, not yet known to us exactly how these torques act in real flows, but it is worth considering that the normal stresses are imposed on the boundary through a boundary layer (Joseph 2003). The analysis here, in any event, can be justified as a way to address the defects of the conventional theory of irrotational flow of an inviscid fluid which also neglects shear, but disallows all the possible effects of viscosity and viscoelasticity on the normal stress.

2. Potential flow over a sphere

The potential of a uniform flow of a second-order fluid past a sphere is given by

$$\phi = -Ur \cos \theta \left(1 + \frac{a^3}{2r^3} \right), \quad (2.1)$$

where U is the velocity of the uniform stream and a is the radius of the sphere. This is a steady flow and the stress (1.8) can be evaluated on (2.1). This has not been done before. The velocities are

$$u_r = -U \left(1 - \frac{a^3}{r^3} \right) \cos \theta, \quad u_\theta = U \left(1 + \frac{a^3}{2r^3} \right) \sin \theta. \tag{2.2}$$

The tensors \mathbf{L} and \mathbf{A} can be evaluated

$$\mathbf{L} = \frac{3a^3U}{2r^4} \begin{bmatrix} -2 \cos \theta & -\sin \theta & 0 \\ -\sin \theta & \cos \theta & 0 \\ 0 & 0 & \cos \theta \end{bmatrix}, \quad \mathbf{A} = 2\mathbf{L}. \tag{2.3}$$

Then the Bernoulli equation (1.7) is used to obtain the pressure at the surface of the sphere

$$p = p_\infty + \left(\frac{27}{2}\alpha_1 + 9\alpha_2 \right) \frac{U^2}{a^2} (1 + 2 \cos^2 \theta) + \frac{1}{2} \rho U^2 (1 - \frac{9}{4} \sin^2 \theta) \tag{2.4}$$

where p_∞ is the pressure at infinity. The normal stress T_{rr} at the surface of the sphere is calculated from (1.8) and expressed in a dimensionless form

$$T_{rr}^* = \frac{T_{rr} + p_\infty}{\rho U^2 / 2} = \left(\frac{9}{4} \sin^2 \theta - 1 \right) - \frac{12}{R_e} \cos \theta + \frac{\alpha_1}{\rho a^2} (36 \sin^2 \theta - 9) + 18 \frac{\alpha_2}{\rho a^2} \cos^2 \theta, \tag{2.5}$$

where $R_e = \rho U a / \mu$ is the Reynolds number. The viscous normal stress should be zero at a solid boundary in a Newtonian fluid or an Oldroyd-B fluid; the viscous effect on the normal stress is hidden in the pressure. The viscous contribution to the pressure at the surface of a sphere in a Stokes flow of Newtonian fluid is (Panton 1984, p. 646)

$$\frac{p - p_\infty}{\rho U^2 / 2} = \frac{3}{R_e} \cos \theta.$$

In (2.5), we have a viscous contribution to the normal stress $(12/R_e) \cos \theta$ which is four times the Stokes value $(3/R_e) \cos \theta$.

We compute the normal stress (2.5) for the liquid M1 with a density $\rho = 0.895 \text{ g cm}^{-3}$, $\alpha_1 = -3$ and $\alpha_2 = 5.34 \text{ g cm}^{-1}$ (Hu *et al.* 1990) as an example. We plot the dimensionless normal stress T_{rr}^* as a function of the angle θ in figure 1.

At the stagnation points of a sphere [$r = a$, $\theta = 0$ or π], the normal stresses are, respectively

$$\frac{T_{rr} + p_\infty}{\rho U^2 / 2} = \left[-1 + \frac{9(2\alpha_2 - \alpha_1)}{\rho a^2} \right] \mp \frac{12}{R_e}. \tag{2.6}$$

The viscous contribution gives rise to compression $-12/R_e$ at the front stagnation point and to tension $12/R_e$ at the rear. The stress due to inertia and viscoelasticity is the same at $\theta = 0$ and $\theta = \pi$ and is a tension when $9(2\alpha_2 - \alpha_1) > \rho a^2$. The quantity $2\alpha_2 - \alpha_1$ is strongly positive; for example, $2\alpha_2 - \alpha_1 = 13.68 \text{ (g cm}^{-1}\text{)}$ for the liquid M1. Hence, if a^2 is not too large, the stress at the stagnation points is a tension, reversing the compression due to inertia.

Figure 1 shows that when viscous effects are dominant ($R_e = 0.05$, $a = 1 \text{ cm}$), the stress is compression at the leading edge and tension at the trailing edge. When the viscoelastic effects are important ($R_e = 1$, $a = 1 \text{ cm}$ and $R_e = 1$, $a = 0.5 \text{ cm}$), the stress is tension at both stagnation points. The normal stress on the sphere with $a = 0.5 \text{ cm}$ is much stronger than that on the sphere with $a = 1 \text{ cm}$, because the viscoelastic effects are proportional to $1/a^2$. The distribution of normal stresses, especially the tension at

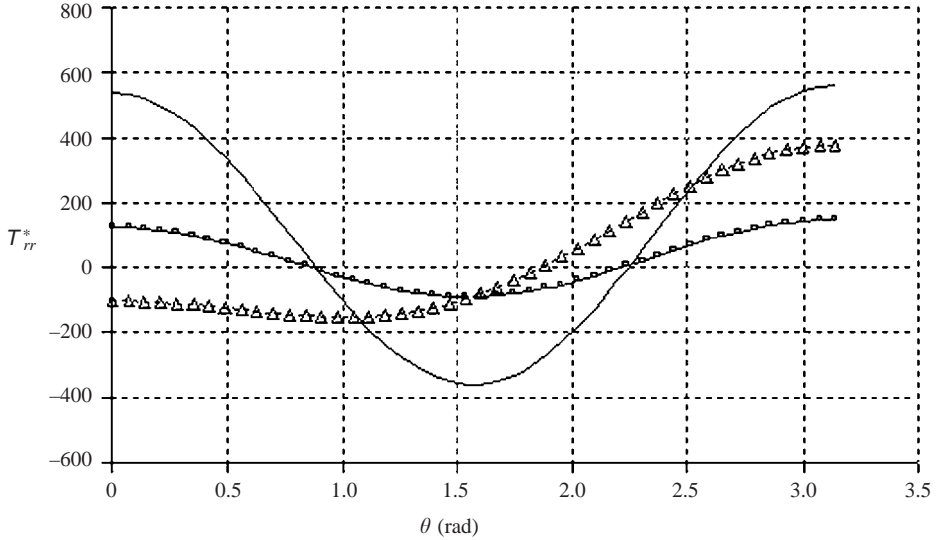


FIGURE 1. The dimensionless normal stress T_{rr}^* as a function of the angle θ . Parameters of the liquid M1 are used in the calculation: $\rho = 0.895 \text{ g cm}^{-3}$, $\alpha_1 = -3$ and $\alpha_2 = 5.34 \text{ g cm}^{-1}$. The three curves in the figure correspond to \square , $R_e = 1$, $a = 1 \text{ cm}$; \triangle , $R_e = 0.05$, $a = 1 \text{ cm}$; and $—$, $R_e = 1$, $a = 0.5 \text{ cm}$, respectively.

the trailing edge, shown in figure 1 is compatible with the cusp shape of gas bubbles rising in viscoelastic fluids (see § 6).

A point of stagnation on a stationary body in potential flow is a unique point at the end of a dividing streamline at which the velocity vanishes. In a viscous fluid all the points on the boundary of a stationary body have a zero velocity but the dividing streamline can be found and it marks the place of zero shear stress near which the velocity is small. The stagnation pressure makes sense even in a viscous fluid where the high pressure of the potential flow outside the boundary layer is transmitted right through the boundary layer to the body. It is a good idea to look for the dividing streamlines where the shear stress vanishes in any analysis of the flow pattern around the body.

3. Potential flow over an ellipse

Potential flow over an ellipse is a classical problem in airfoil theory. The solutions are most easily expressed in terms of complex functions of a complex variable (Lamb 1932; Milne-Thomson 1968). Hence, we shall use this potential flow solution and obtain the pressure and the normal stress for a second-order fluid as a composition of the derivatives of that solution. Two-dimensional potential flows around bodies admit the addition of circulation which we have here put to zero.

The complex potential for the flow over an ellipse given by

$$\frac{x^2}{a^2} + \frac{y^2}{b^2} = 1 \quad (3.1)$$

is (Milne-Thomson 1968, § 6.31)

$$\omega = -\frac{1}{2}U(a+b) \left[\frac{e^{-i\alpha}(z + \sqrt{z^2 - c^2})}{a+b} + \frac{e^{i\alpha}(z - \sqrt{z^2 - c^2})}{a-b} \right], \quad (3.2)$$

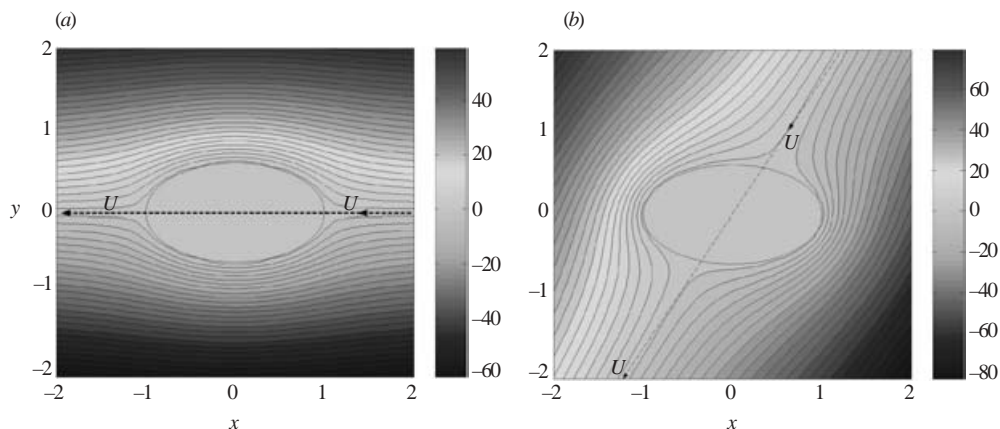


FIGURE 2. The streamlines of the flow over an ellipse. (a) The angle of attack $\alpha = 0^\circ$; (b) $\alpha = 60^\circ$.

where z is the complex variable, α is the angle of attack, a and b are the semi-axes of the ellipse and $c^2 = a^2 - b^2$. We plot the streamlines of the flow with the angle of attack $\alpha = 0^\circ$ and 60° in figure 2.

The velocities are

$$u = \frac{1}{2} \left(\frac{d\omega}{dz} + \frac{d\bar{\omega}}{d\bar{z}} \right), \quad v = \frac{i}{2} \left(\frac{d\omega}{dz} - \frac{d\bar{\omega}}{d\bar{z}} \right). \tag{3.3}$$

$$\mathbf{L} = \nabla \mathbf{u} = \begin{bmatrix} \partial u / \partial x & \partial v / \partial x \\ \partial u / \partial y & \partial v / \partial y \end{bmatrix}, \quad \mathbf{A} = \mathbf{L} + \mathbf{L}^T = \begin{bmatrix} n & s \\ s & -n \end{bmatrix}, \tag{3.4}$$

where $n = d^2\omega/dz^2 + d^2\bar{\omega}/d\bar{z}^2$ and $s = i((d^2\omega/dz^2) - (d^2\bar{\omega}/d\bar{z}^2))$. It follows that

$$\mathbf{A}^2 = (n^2 + s^2)\mathbf{1}, \quad \text{tr} \mathbf{A}^2 = 2(n^2 + s^2). \tag{3.5}$$

Letting U and p_∞ be the velocity and pressure at infinity, respectively, we find the pressure by (1.7)

$$p = p_\infty + \frac{1}{2}\rho U^2 - \frac{1}{2}\rho \frac{d\omega}{dz} \frac{d\bar{\omega}}{d\bar{z}} + (3\alpha_1 + 2\alpha_2)(n^2 + s^2)/2. \tag{3.6}$$

The stress can then be calculated using (1.8); after some arrangement, we find

$$\begin{aligned} \mathbf{T} = & \left[-p_\infty - \frac{1}{2}\rho U^2 + \frac{1}{2}\rho \frac{d\omega}{dz} \frac{d\bar{\omega}}{d\bar{z}} - \frac{1}{2}\alpha_1(n^2 + s^2) \right] \mathbf{1} \\ & + \mu \begin{bmatrix} n & s \\ s & -n \end{bmatrix} + \alpha_1 u \begin{bmatrix} k & q \\ q & -k \end{bmatrix} + \alpha_1 v \begin{bmatrix} q & -k \\ -k & -q \end{bmatrix}, \end{aligned} \tag{3.7}$$

where $k = d^3\omega/dz^3 + d^3\bar{\omega}/d\bar{z}^3$ and $q = i((d^3\omega/dz^3) - (d^3\bar{\omega}/d\bar{z}^3))$. Equation (3.7) applies to any two-dimensional flow that can be represented by a complex potential ω . Note that α_2 does not appear in the expression for the stress in two-dimensional cases, which has been reported in Joseph 1992*b*.

We are interested in the normal stress on the surface of the ellipse. The unit normal vector on the surface is

$$\mathbf{n} = \frac{(x/a^2)\mathbf{e}_x + (y/b^2)\mathbf{e}_y}{(x^2/a^4 + y^2/b^4)^{1/2}}. \tag{3.8}$$

The normal stress is calculated from $T_{nn} = \mathbf{n} \cdot \mathbf{T} \cdot \mathbf{n}$.

4. Normal stress at the surface of the ellipse

We present the results for the normal stress on the ellipse in this section. Besides the angle of attack, there are six relevant parameters: ρ , U , μ , a , b and α_1 in this problem. Three dimensionless parameters can be constructed:

$$R_e = \frac{\rho U a}{\mu}, \quad \frac{-\alpha_1}{\rho a^2}, \quad \frac{a}{b}. \quad (4.1)$$

Note that the Deborah number can be defined as $D_e = (-\alpha_1/\mu)(U/a)$ and $-\alpha_1/\rho a^2 = D_e/R_e$. We shall see later that the parameter $-\alpha_1/(\rho a^2)$ appears in the expressions for the normal stresses at the stagnation points. Therefore, we use the parameter $-\alpha_1/(\rho a^2)$ rather than the Deborah number. The dimensionless normal stress is

$$T_{nn}^* = \frac{T_{nn} + p_\infty}{\frac{1}{2}\rho U^2}. \quad (4.2)$$

The effects of the three dimensionless parameters on the normal stress at the surface of the ellipse are studied in flows of a zero attack angle. We can obtain explicit expressions for the normal stresses at the stagnation points, from which the effects of the three parameters can be understood readily. Such expressions are not obtained for an arbitrary point on the ellipse surface, instead, we calculate the numerical values of stress and present the plots for the distribution of the normal stress.

At the front stagnation point where $z = a$, we have

$$u = v = 0, \quad n = -2U(a+b)/b^2, \quad s = 0. \quad (4.3)$$

Inserting (4.3) into (3.7) and noting that $T_{nn} = T_{xx}$, we obtain the dimensionless normal stress at the front stagnation point

$$T_{nn}^*(\theta = 0) = -1 + \frac{-\alpha_1}{\rho a^2} 4 \left(1 + \frac{b}{a}\right)^2 \frac{a^4}{b^4} - \frac{4}{R_e} \left(1 + \frac{b}{a}\right) \frac{a^2}{b^2}. \quad (4.4)$$

Similarly, we can find the dimensionless normal stress at the rear stagnation point

$$T_{nn}^*(\theta = \pi) = -1 + \frac{-\alpha_1}{\rho a^2} 4 \left(1 + \frac{b}{a}\right)^2 \frac{a^4}{b^4} + \frac{4}{R_e} \left(1 + \frac{b}{a}\right) \frac{a^2}{b^2}. \quad (4.5)$$

The difference between the two stresses is

$$T_{nn}^*(\theta = \pi) - T_{nn}^*(\theta = 0) = \frac{8}{R_e} \left(1 + \frac{b}{a}\right) \frac{a^2}{b^2}. \quad (4.6)$$

The normal stresses (4.4) and (4.5) are analogous to the normal stress (2.6) at the stagnation points in the sphere case, in the sense that they are all composed of the inertia, viscous and viscoelastic terms. Here, the viscoelastic term $(-\alpha_1/\rho a^2)4(1+b/a)^2 a^4/b^4$ gives rise to extension at both of the stagnation points; the viscous term $(4/R_e)(1+b/a)a^2/b^2$ leads to compression at the front stagnation point and tension at the rear stagnation point.

4.1. The effects of the Reynolds number

We calculate the normal stress at the surface of the ellipse in flows where $-\alpha_1/(\rho a^2)$ and a/b are fixed at 3 and 1.67, respectively, and the Reynolds number changes from 0.01 to 100. In figure 3, we plot T_{nn}^* at the front and rear stagnation points as functions of the Reynolds number. The stress at the front stagnation point changes from

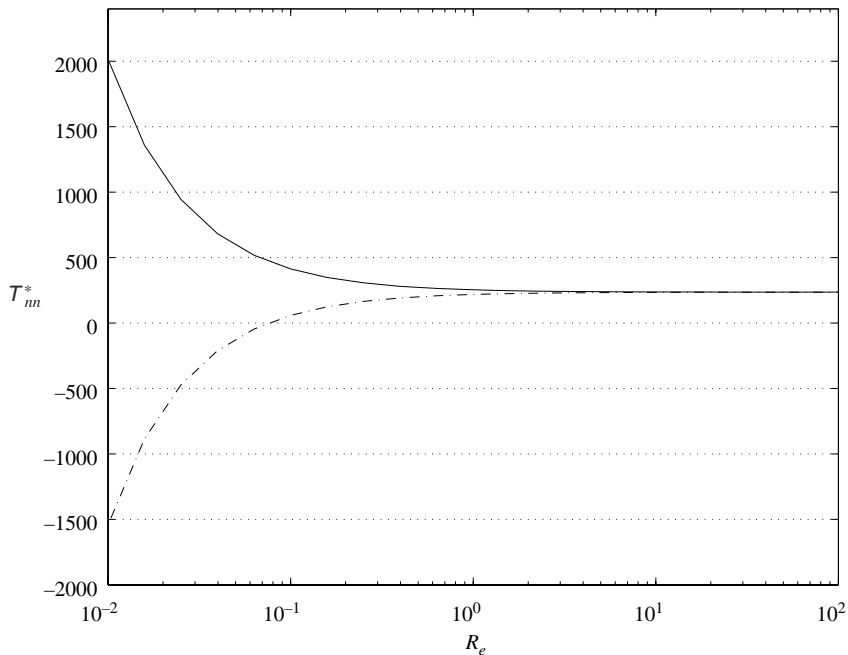


FIGURE 3. The dimensionless normal stresses T_{nn}^* at the \cdots -, front and --- -, rear stagnation points as functions of the Reynolds number. The other two parameters are fixed: $-\alpha_1/(\rho a^2) = 3$ and $a/b = 1.67$.

compression to extension as the Reynolds number increases. The critical Reynolds number, at which $T_{nn}^* = 0$ at the front stagnation point, is 0.075, as shown in figure 3. Equation (4.6) indicates that the difference between the two normal stresses vanishes as the Reynolds number tends to infinity; the asymptotic value of the two stresses is

$$T_{nn}^* \left(R_e \rightarrow \infty, \frac{-\alpha_1}{\rho a^2} = 3, \frac{a}{b} = 1.67 \right) = 236.07.$$

The distribution of the normal stress at the surface is plotted in figure 4 for flows with Reynolds numbers 0.05 and 1. We notice that the stress is compression at the front stagnation point and extension at the rear stagnation point when $R_e = 0.05$; however, the stress is tension at both of the stagnation points when $R_e = 1$.

4.2. The effects of $-\alpha_1/(\rho a^2)$

The two normal stresses at stagnation points are plotted against the parameter $-\alpha_1/(\rho a^2)$ in figure 5; the other two parameters are fixed: $R_e = 0.1$ and $a/b = 1.67$. The difference between the two stresses is independent of the parameter $-\alpha_1/(\rho a^2)$, as can be seen from (4.6). This difference is 355.6 when $R_e = 0.1$ and $a/b = 1.67$. The critical value of $-\alpha_1/(\rho a^2)$, at which $T_{nn}^* = 0$ at the front stagnation point, is 2.26.

4.3. The effects of the aspect ratio

We change the aspect ratio from 1.1 to 10 and compute the normal stress on the surface of the ellipse; the other two parameters are fixed: $R_e = 0.1$ and $-\alpha_1/(\rho a^2) = 3$. The two stresses at the stagnation points are plotted against the aspect ratio in

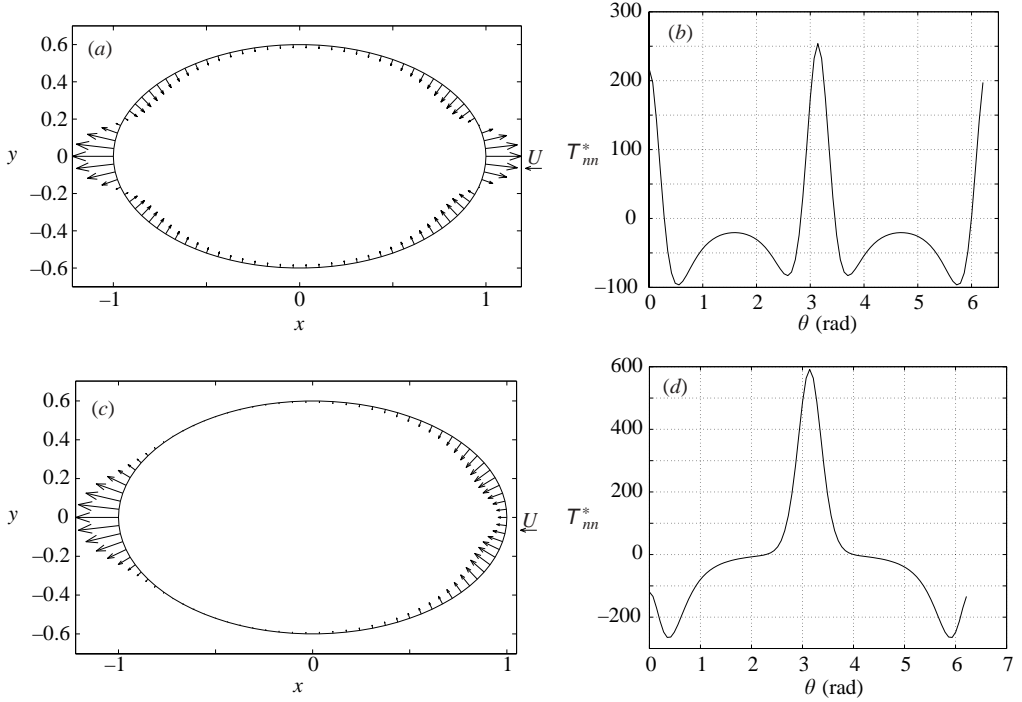


FIGURE 4. The distribution of the dimensionless normal stress T_{nn}^* at the surface of the ellipse in flows with $-\alpha_1/(\rho a^2) = 3$ and $a/b = 1.67$. The Reynolds number is 1.0 in (a) and (b), and is 0.05 in (c) and (d). The normal stress is represented by vectors at the surface of the ellipse in (a) and (c), and is plotted against the polar angle θ in (b) and (d).

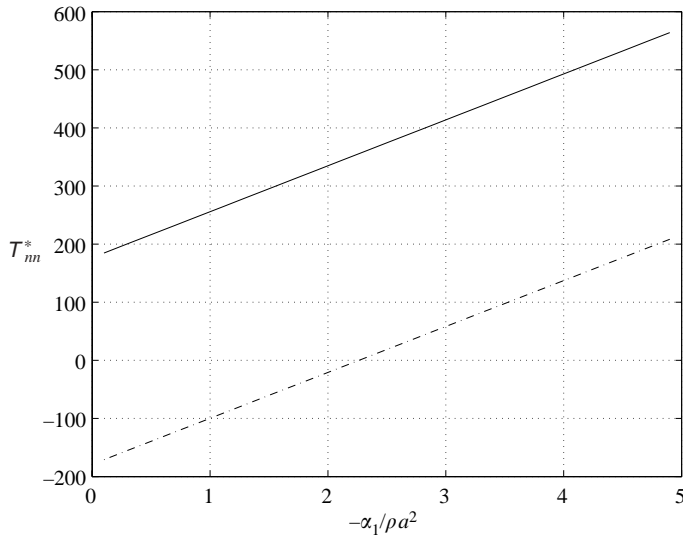


FIGURE 5. The dimensionless normal stresses T_{nn}^* at the front $---$, and $—$, rear stagnation points as functions of the parameter $-\alpha_1/(\rho a^2)$. The other two parameters are fixed: $R_e = 0.1$ and $a/b = 1.67$.

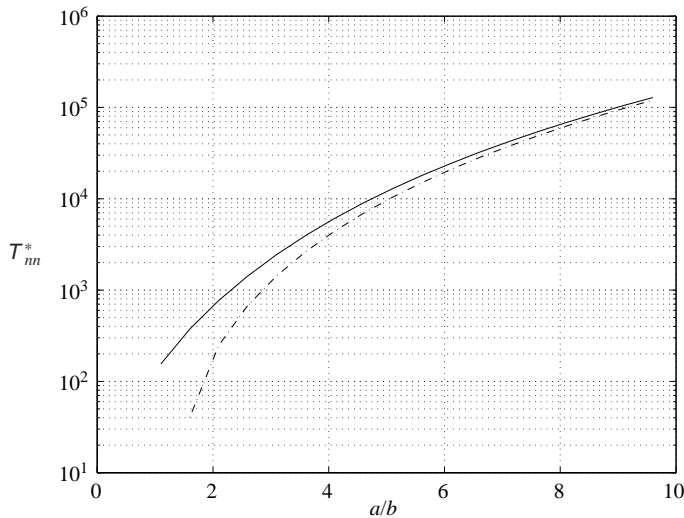


FIGURE 6. The dimensionless normal stresses T_{nn}^* at the $- \cdot -$, front and $-$, rear stagnation points as functions of the aspect ratio a/b . The other two parameters are fixed: $Re = 0.1$ and $-\alpha_1/(\rho a^2) = 3$.

figure 6; The values of the stresses change dramatically with the aspect ratio because of the a^4/b^4 term in (4.4) and (4.5). The stress at the front stagnation point changes from compression to extension as a/b increases; when $a/b = 1.40$, $T_{nn}^* = 0$ at the front stagnation point. (The negative values are not shown on the semi-log plot in figure 6).

The normal stress distribution at the surface is plotted in figure 7 for flows with $a/b = 5.0$ and 1.1 . It can be seen that in the flow with the higher aspect ratio, the ellipse is under very high extensional stresses at both of the stagnation points. The stress at the front stagnation point is compression when $a/b = 1.1$, which implies that the front nose of a gas bubble will be flattened.

5. The moment on the ellipse

Long bodies falling in a viscoelastic fluid often turn into the streamwise direction (Liu & Joseph 1993). We calculate the dimensionless moment by the normal stress on the ellipse

$$M^* = \frac{M}{\frac{1}{2}\rho U^2 a^2} = \frac{\oint \mathbf{x} \wedge (T_{nn}\mathbf{n}) dl}{\frac{1}{2}\rho U^2 a^2}. \tag{5.1}$$

In a Newtonian fluid, the moment can be calculated using the theorem of Blasius and the dimensionless moment is

$$M^* = -2\pi(1 - a^2/b^2) \sin \alpha \cos \alpha, \tag{5.2}$$

which does not depend on the Reynolds number. Our calculation shows that the conclusion is also true in a second-order fluid: the dimensionless moment does not depend on the Reynolds number; the parameter $-\alpha_1/(\rho a^2)$ and the aspect ratio a/b are relevant parameters when the moment is concerned.

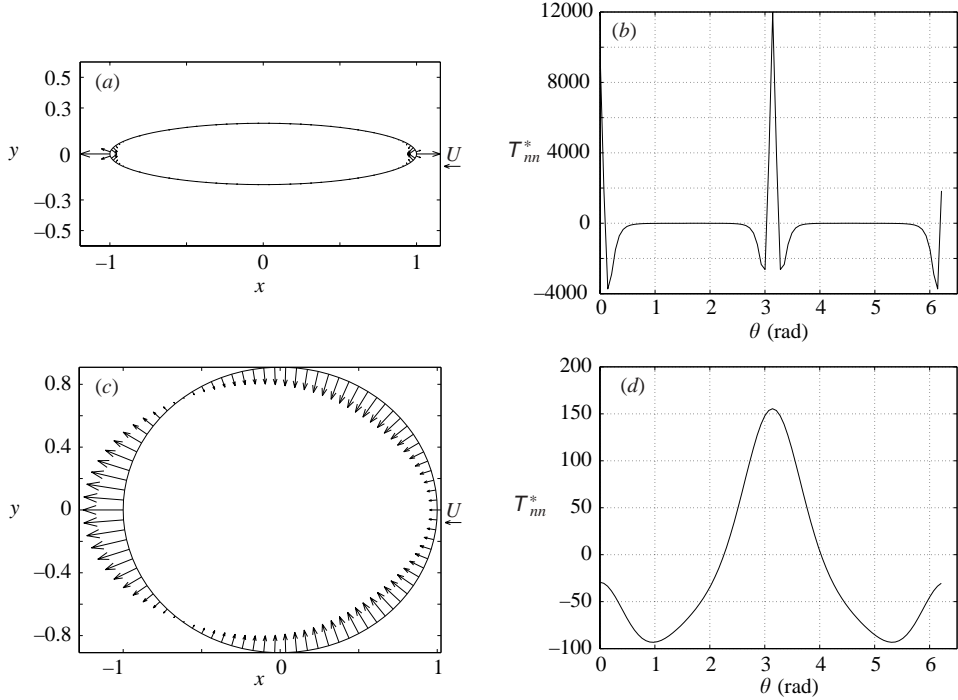


FIGURE 7. The distribution of the dimensionless normal stress T_{nn}^* at the surface of the ellipse in flows with $R_e = 0.1$ and $-\alpha_1/(\rho a^2) = 3$. The aspect ratio is 5.0 in (a) and (b), and is 1.1 in (c) and (d). The normal stress is represented by vectors at the surface of the ellipse in (a) and (c), and is plotted against the polar angle θ in (b) and (d).

We plot the dimensionless moment on the ellipse by the normal stress as a function of the attack angle α in the range $[0, \pi/2]$ in figure 8. Six values of the parameter $-\alpha_1/(\rho a^2)$, from 0 to 5, are investigated. The curve corresponding to $-\alpha_1/(\rho a^2) = 0$ in figure 8 is in agreement with (5.2), which is the moment in a Newtonian fluid. The moment on the ellipse is negative in a Newtonian fluid and turns the ellipse broadside-on to the stream (see figure 9a). When the parameter $-\alpha_1/(\rho a^2)$ is larger, the moment on the ellipse becomes positive and tends to align the broad side of the ellipse with the streamwise direction (see figure 9b). Figure 8 shows that the magnitude of the moment reaches its largest value when $\alpha = \pi/4$, which also occurs in a Newtonian fluid.

We show the effects of the aspect ratio on the moment in figure 10. The five curves correspond to five values of the aspect ratio a/b : 1.1, 4, 6, 8 and 10; the parameter $-\alpha_1/(\rho a^2)$ is fixed at 3. It can be seen that as the aspect ratio increases, the magnitude of the moment increases to huge values. Hence, long slim bodies turn into the streamwise direction quickly in viscoelastic fluids.

6. The reversal of the sign of the normal stress at stagnation points

In §§2 and 4, we have shown that the normal stresses at the stagnation points on a sphere or an ellipse in a second-order fluid can be tension, opposite to the high compressive pressures at the stagnation points in Newtonian fluid. This reversal of

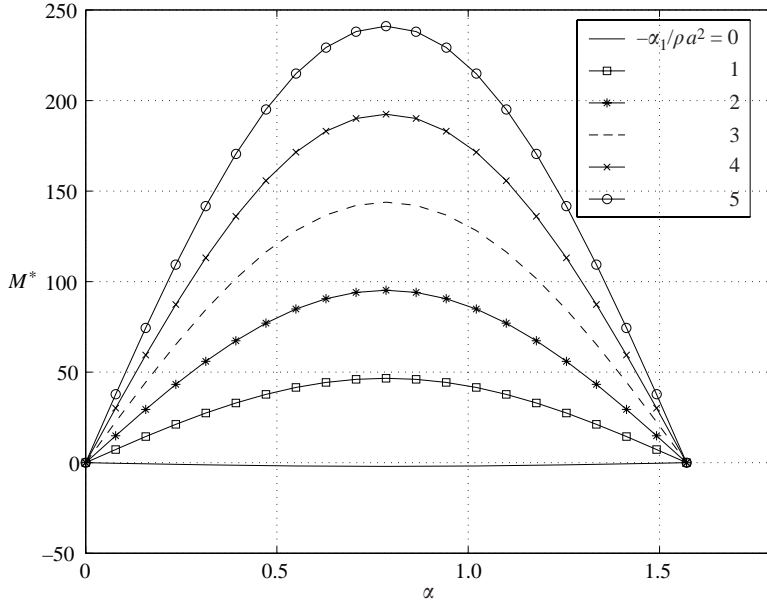


FIGURE 8. The moment on the ellipse by the normal stress as a function of the attack angle α in the range $[0, \pi/2]$. The six curves correspond to six values of the parameter $-\alpha_1/(\rho a^2)$: 0, 1, 2, 3, 4 and 5; the aspect ratio is fixed at $a/b = 1.67$.

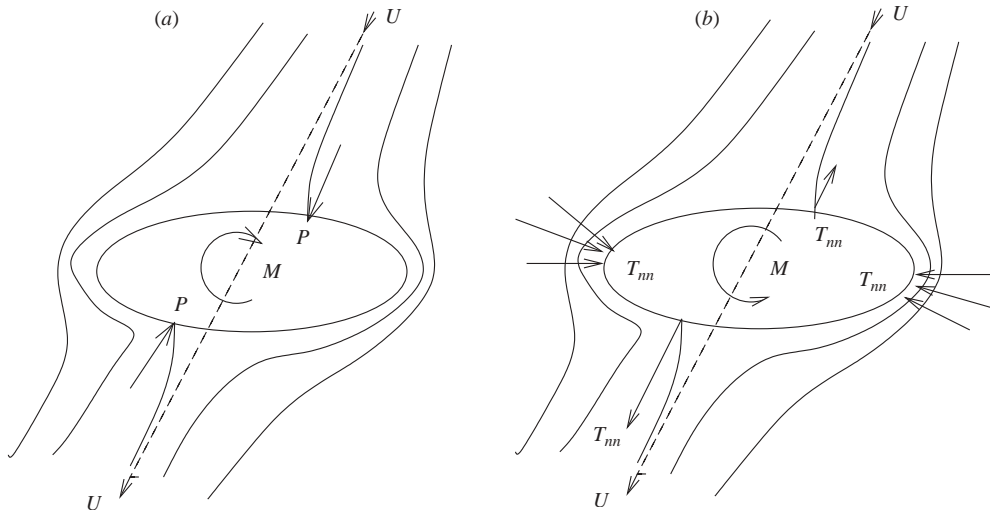


FIGURE 9. The moment on the ellipse in potential flow. (a) In an inviscid fluid, the high pressures at the stagnation points turn the ellipse broadside-on (across the stream); (b) In a second-order fluid, the normal stresses at the two edges where the streamlines are most crowded are compressive and tend to turn the ellipse into the stream. At the two stagnation points, the stresses may change from compression to tension. Here, we illustrate the situation in which the stress is extensional at both of the stagnation points; this pair of stresses gives rise to the moment which tends to turn the ellipse into the stream. Our calculation shows that the resultant moment of the normal stress tends to turn the broad side of the ellipse into the stream when inertia is not dominant.

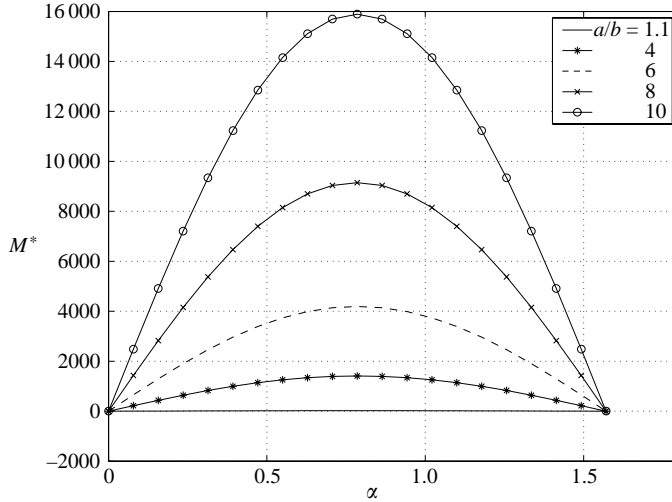


FIGURE 10. The moment on the ellipse by the normal stress as a function of the attack angle α in the range $[0, \pi/2]$. The five curves correspond to five values of the aspect ratio $a/b = 1.1, 4, 6, 8$ and 10 ; the parameter $-\alpha_1/(\rho a^2)$ is fixed at 3 .

the sign of the normal stress has significant effects on the behaviour of particles and bubbles in Newtonian and viscoelastic fluids.

In Newtonian fluids, long bodies in a uniform flow are turned to the orientation in which their long or broad sides are perpendicular to the stream by the high pressures at stagnation points (see figure 9a). This mechanism also determines the stable configurations of suspensions of spherical bodies in Newtonian liquids. Spherical bodies interact and form long bodies momentarily which are unstable to the same turning moment that turns long bodies broadside-on. This implies that globally, the only stable configuration is the one in which the most probable orientation between any pair of neighbouring spheres is across the stream. The consequence of this microstructural property is a flow-induced anisotropy, which leads ubiquitously to lines of spheres across the stream; these are always in evidence in two-dimensional fluidized beds of finite size spheres (Joseph 1996, 2000, chap. 7). Though they are less stable, planes of spheres in three-dimensional beds can also be found.

In viscoelastic fluids, long bodies in a uniform flow often turn into the streamwise direction as we discussed in §5 (see also Liu & Joseph 1993; Joseph & Feng 1996; Huang, Hu & Joseph 1997). The extensional normal stresses at the stagnation points in viscoelastic fluids contribute to the moment which turns the long bodies into the stream (see figure 9b). Long chains of spherical bodies parallel with the stream are in evidence in sedimentation and fluidization flows of viscoelastic fluids; such configurations are opposite to those observed in Newtonian fluids. Another unusual phenomenon in viscoelastic fluids is the two-dimensional cusp at the trailing edge of a rising air bubble (Liu, Liao & Joseph 1995). Below a critical capillary number, an air bubble rising in a viscoelastic fluid adopts the shape with a cusp point in one view and a spade edge in the orthogonal view. Figures 1, 4(c) and 7(c) show situations in which the normal stress is compression at the leading edge and tension at the trailing edge; the leading edge is flattened and the trailing edge is extended, tending to the cusped trailing edge observed in experiments. Our calculation on a smooth sphere

or an ellipse cannot lead to the exact cusp shape. However, the calculation shows that the normal stress computed on viscoelastic potential agrees with the experiment qualitatively, much better than the pressure which is the only normal force that can act on the body in inviscid potential flow.

7. Flow past a flat plate

The flow past an ellipse degenerates to the flow past a flat plate when $b = 0$. The complex potential is

$$\omega = \begin{cases} -U(z \cos \alpha - i\sqrt{z^2 - a^2} \sin \alpha) & \text{upstream to the plate} \\ -U(z \cos \alpha + i\sqrt{z^2 - a^2} \sin \alpha) & \text{downstream to the plate.} \end{cases} \quad (7.1)$$

The velocities at the upper and lower surfaces of the plate are, respectively

$$u = \begin{cases} -U \left(\cos \alpha - \frac{x \sin \alpha}{\sqrt{a^2 - x^2}} \right), & v = 0, \quad \text{upper surface;} \\ -U \left(\cos \alpha + \frac{x \sin \alpha}{\sqrt{a^2 - x^2}} \right), & v = 0, \quad \text{lower surface.} \end{cases} \quad (7.2)$$

The stagnation points at the upper and lower surfaces are $x = a \cos \alpha$ and $x = -a \cos \alpha$, respectively. The dimensionless normal stresses at the two stagnation points are

$$\frac{T_{nn} + p_\infty}{\frac{1}{2}\rho U^2}(x = a \cos \alpha) = -1 + \frac{-\alpha_1}{\rho a^2} \frac{4}{\sin^4 \alpha} - \frac{4}{R_e \sin^2 \alpha}, \quad (7.4)$$

$$\frac{T_{nn} + p_\infty}{\frac{1}{2}\rho U^2}(x = -a \cos \alpha) = -1 + \frac{-\alpha_1}{\rho a^2} \frac{4}{\sin^4 \alpha} + \frac{4}{R_e \sin^2 \alpha}. \quad (7.5)$$

These stresses are degenerate cases of (4.4) and (4.5), which are the stresses at stagnation points in the flow past an ellipse. In (7.4) and (7.5), the viscoelastic term $(-\alpha_1/\rho a^2)(4/\sin^4 \alpha)$ gives rise to extension at both of the stagnation points; the viscous term $(4/R_e)(1/\sin^2 \alpha)$ leads to compression at the front stagnation point and extension at the rear stagnation point.

8. Flow past a circular cylinder with circulation

The complex potential for the flow past a circular cylinder with circulation is (Milne-Thomson 1968, § 7.12)

$$\omega = -U(z + a^2/z) - i\kappa \log(z/a), \quad (8.1)$$

where κ is the strength of the circulation. A dimensionless parameter κ/aU can be introduced.

We calculate the stress using the potential (8.1) in a second-order fluid. The stresses at the surface of the cylinder, where $z = ae^{i\theta}$, are of interest. We find

$$u = -\sin \theta(2U \sin \theta + \kappa/a), \quad v = \cos \theta(2U \sin \theta + \kappa/a), \quad (8.2)$$

$$n = -4U \cos 3\theta/a + 2\kappa \sin 2\theta/a^2, \quad s = -(4U \sin 3\theta/a + 2\kappa \cos 2\theta/a^2), \quad (8.3)$$

$$k = 12U \cos 4\theta/a^2 - 4\kappa \sin 3\theta/a^3, \quad q = 12U \sin 4\theta/a^2 + 4\kappa \cos 3\theta/a^3, \quad (8.4)$$

at $z = ae^{i\theta}$ and the stress tensor is obtained by inserting (8.2)–(8.4) into (3.7). The dimensionless normal stress is given by

$$\begin{aligned} \frac{T_{nn} + p_\infty}{\frac{1}{2}\rho U^2} = & \left[-1 + 4 \sin^2 \theta + \left(\frac{\kappa}{aU} \right)^2 + \frac{\kappa}{aU} 4 \sin \theta \right] - \frac{8}{R_e} \cos \theta \\ & + \frac{4\alpha_1}{\rho a^2} \left[-4 + 12 \sin^2 \theta + \left(\frac{\kappa}{aU} \right)^2 + \frac{\kappa}{aU} 6 \sin \theta \right], \quad (8.5) \end{aligned}$$

where the first term on the right-hand side is the inertia term, which is the same as the inviscid pressure; the second term is the viscous term and the third term is the viscoelastic term.

The force and moment on the cylinder can be obtained by direct integration of the normal stress over the surface of the cylinder:

$$F_x = \int_0^{2\pi} T_{nn} \cos \theta a \, d\theta = -4\pi\mu U, \quad (8.6)$$

$$F_y = \int_0^{2\pi} T_{nn} \sin \theta a \, d\theta = 2\pi\kappa U (\rho + 6\alpha_1/a^2). \quad (8.7)$$

The moment is obviously zero. Equation (8.6) shows that the cylinder experiences a drag due to the viscosity; the drag would be zero if the shear stress were included in the integration. Equation (8.7) shows that the lift has a contribution from the viscoelastic effect in addition to the inviscid lift $2\pi\kappa\rho U$. Since α_1 is negative, the viscoelastic lift is opposite to the inviscid lift. When $-\alpha_1/(\rho a^2) = 1/6$, the total lift force is zero.

9. Conclusions

We use viscoelastic potential flow to study a uniform flow of a second-order fluid past a sphere. The normal stress at the surface of the body is evaluated on the potential and has contributions from inertia, viscous and viscoelastic effects. The viscous term is proportional to $1/R_e$ and the viscoelastic term is proportional to $1/a^2$.

Viscoelastic potential flow of a second-order fluid over an ellipse is also studied. We present explicit expressions for the normal stresses at the two stagnation points on the ellipse. In both the sphere and the ellipse cases, the viscoelastic term in the normal stress gives rise to extension at both of the stagnation points; the viscous term leads to compression at the front stagnation point and extension at the rear stagnation point. The normal stresses at the stagnation points can be tension, opposite to the high compressive pressures at the stagnation points in Newtonian fluid. This reversal of the sign of the normal stress causes long bodies to turn into the stream and causes spherical bodies to chain; it could also offer a qualitative explanation of the cusped trailing edge of an air bubble rising in viscoelastic fluids observed in experiments.

We calculate the normal stress distribution on the surface of the ellipse; the effects of the Reynolds number, the viscoelastic parameter $-\alpha_1/(\rho a^2)$ and the aspect ratio a/b are investigated. The resultant moment of the normal stress on the ellipse is calculated; the moment when viscoelastic effect is important is opposite to that in Newtonian fluids. This moment is very large when the aspect ratio is large, indicating the long slim bodies will turn into the stream very quickly.

The flow past a flat plate is discussed as a degenerate case of the ellipse. Circulation is considered for the flow past a circular cylinder. The force and moment on the

cylinder can be obtained by direct integration of the normal stress over the surface of the cylinder. The moment is zero and the viscoelastic lift is opposite to the lift calculated from the inviscid potential flow.

This work was supported in part by the NSF under grants from Chemical Transport Systems and the DOE (engineering research program of the Department of Basic Engineering Sciences).

REFERENCES

- BIRD, R., ARMSTRONG, R. & HASSAGER, O. 1987 *Dynamics of Polymeric Liquids*. John Wiley.
- HU, H. H., RICCIUS, O., CHEN, K. P., ARNEY, M. & JOSEPH, D. D. 1990 Climbing constant, second-order correction of Trouton's viscosity, wave speed and delayed die swell for M1. *J. Non-Newtonian Fluid Mech.* **35**, 287–307.
- HUANG, P. Y., HU, H. H. & JOSEPH, D. D. 1997 Direct simulation of the sedimentation of elliptical particles in Oldroyd-B fluids. *J. Fluid Mech.* **362**, 297–325.
- JOSEPH, D. D. 1990 *Dynamics of Viscoelastic Liquids*. Springer.
- JOSEPH, D. D. 1992a Bernoulli equation and the competition of elastic and inertial pressure in the potential flow of a second-order fluid. *J. Non-Newtonian Fluid Mech.* **42**, 385–389.
- JOSEPH, D. D. 1992b Understanding cusped interfaces. *J. Non-Newtonian Fluid Mech.* **44**, 127–148.
- JOSEPH, D. D. 1996 Flow induced microstructure in Newtonian and viscoelastic fluids. In *Proc. 5th World Congress of Chem. Engng, Particle Technology Track, San Diego, 14–18 July*. AIChE vol. 6, pp. 3–16.
- JOSEPH, D. D. 2000 Interrogation of direct numerical simulation of solid–liquid flow. Available at <http://www.efluids.com/efluids/books/joseph.htm>.
- JOSEPH, D. D. 2003 Viscous potential flow. *J. Fluid Mech.* **479**, 191–197.
- JOSEPH, D. D. & FENG, J. 1996 A note on the forces that move particles in a second-order fluid. *J. Non-Newtonian Fluid Mech.* **64**, 299–302.
- JOSEPH, D. D. & LIAO, T. Y. 1994a Potential flows of viscous and viscoelastic fluids. *J. Fluid Mech.* **265**, 1–23.
- JOSEPH, D. D. & LIAO, T. Y. 1994b Viscous and viscoelastic potential flow. In *Trends and Perspectives in Applied Mathematics*, vol. 100 (ed. L. Sirovich). Springer.
- JOSEPH, D. D. & WANG, J. 2004 The dissipation approximation and viscous potential flow. *J. Fluid Mech.* **505**, 365–377.
- LAMB, H. 1932 *Hydrodynamics*, 6th edn. Cambridge University Press. (Reprinted by Dover, 1945.)
- LIU, Y. J. & JOSEPH, D. D. 1993 Sedimentation of particles in polymer solutions. *J. Fluid Mech.* **255**, 565–595.
- LIU, Y. J., LIAO, T. Y. & JOSEPH, D. D. 1995 A two-dimensional cusp at the trailing edge of an air bubble rising in a viscoelastic liquid. *J. Fluid Mech.* **304**, 321–342.
- MILNE-THOMSON, L. M. 1968 *Theoretical Hydrodynamics*. Macmillan.
- PANTON, R. 1984 *Incompressible Flow*. John Wiley.
- RIVLIN, R. S. & ERICKSEN, J. L. 1955 Stress deformation relations for isotropic materials. *J. Rat. Mech. Anal.* **4**, 323–425.